Supporting Information

Mechanistic Understanding of Metal Phosphide Host for Sulfur Cathode in High-Energy-Density Lithium-Sulfur Batteries

Jiadong Shen,[†] Xijun Xu,[†] Jun Liu,[†,*] Zhengbo Liu,[†] Fangkun Li,[†] Renzong Hu,[†]

Jiangwen Liu,[†] Xianhua Hou,[§] Yuezhan Feng,[‖] Yan Yu[‡,&*], and Min Zhu[†,*]

[†]School of Materials Science and Engineering and Guangdong Provincial Key Laboratory of Advanced Energy Storage Materials, South China University of Technology, Guangzhou, 510641, PR China

E-mail: msjliu@scut.edu.cn; memzhu@scut.edu.cn

[‡] Hefei National Laboratory for Physical Sciences at the Microscale, Department of Materials Science and Engineering, Key Laboratory of Materials for Energy Conversion, Chinese Academy of Sciences, University of Science and Technology of China, Hefei, Anhui, 230026, China. E-mail: yanyumse@ustc.edu.cn

[§]Guangdong Provincial Key Laboratory of Quantum Engineering and Quantum Materials, School of Physics and Telecommunication Engineering, South China Normal University, Guangzhou 510006, PR China

[‖]Key Laboratory of Materials Processing and Mold (Zhengzhou University), Ministry of Education, Zhengzhou University, Zhengzhou 450002, China

[&]State Key Laboratory of Fire Science, University of Science and Technology of China, Hefei, Anhui, 230026, China.
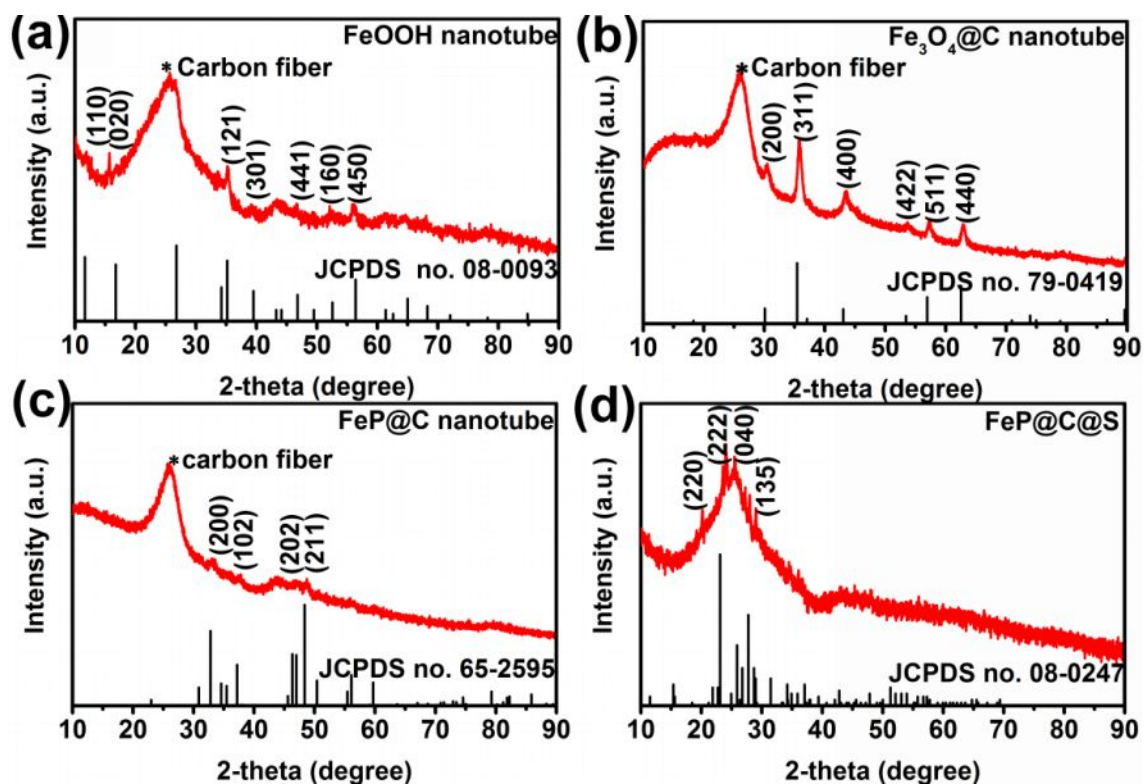
Figure S1. XRD patterns for self-supported films of FeOOH (a), Fe$_3$O$_4$@C (b), FeP@C (c) and FeP@C@S (d) nanotube arrays grown on CF substrate.
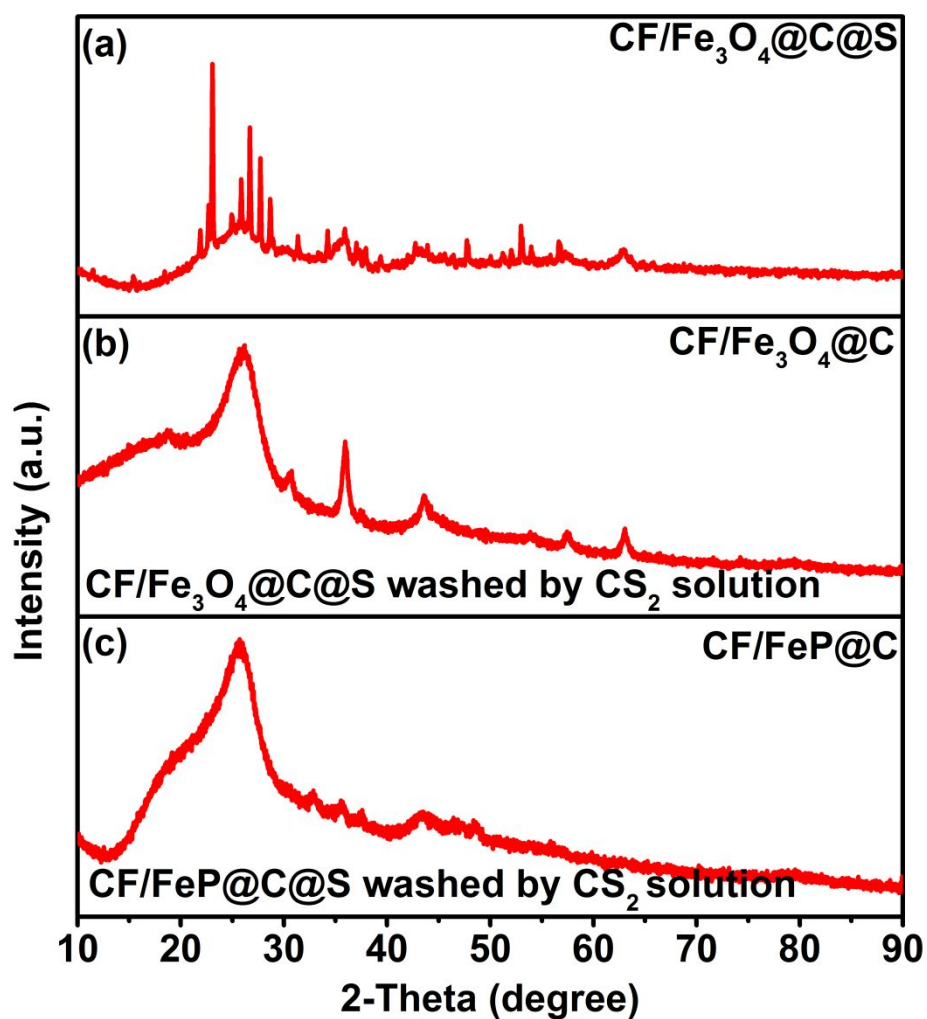
Figure S2. XRD patterns of CF/Fe$_3$O$_4$@C@S (a) CF/Fe$_3$O$_4$@C (b) and CF/FeP@C (c).

CF/Fe$_3$O$_4$@C and CF/FeP@C used for XRD testing were obtained by dissolving the

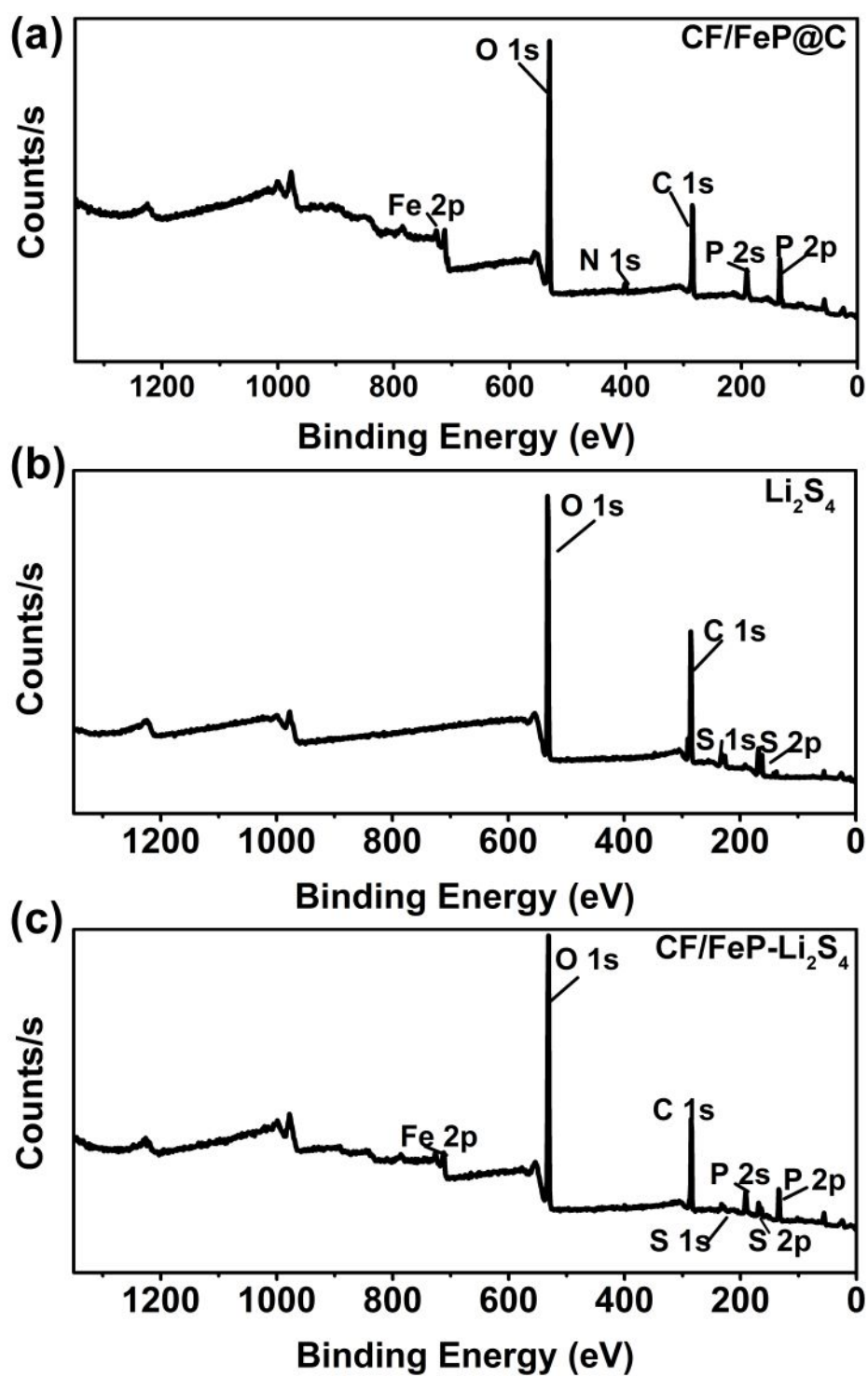sulfur *via* immersing the CF/Fe$_3$O$_4$@C@S and CF/FeP@C@S into CS$_2$ solution.

Figure S3. XPS survey-level scan spectra of CF/FeP@C (a), Li_2S_4 powder (b) and CF/FeP@C-Li_2S_4 (c).
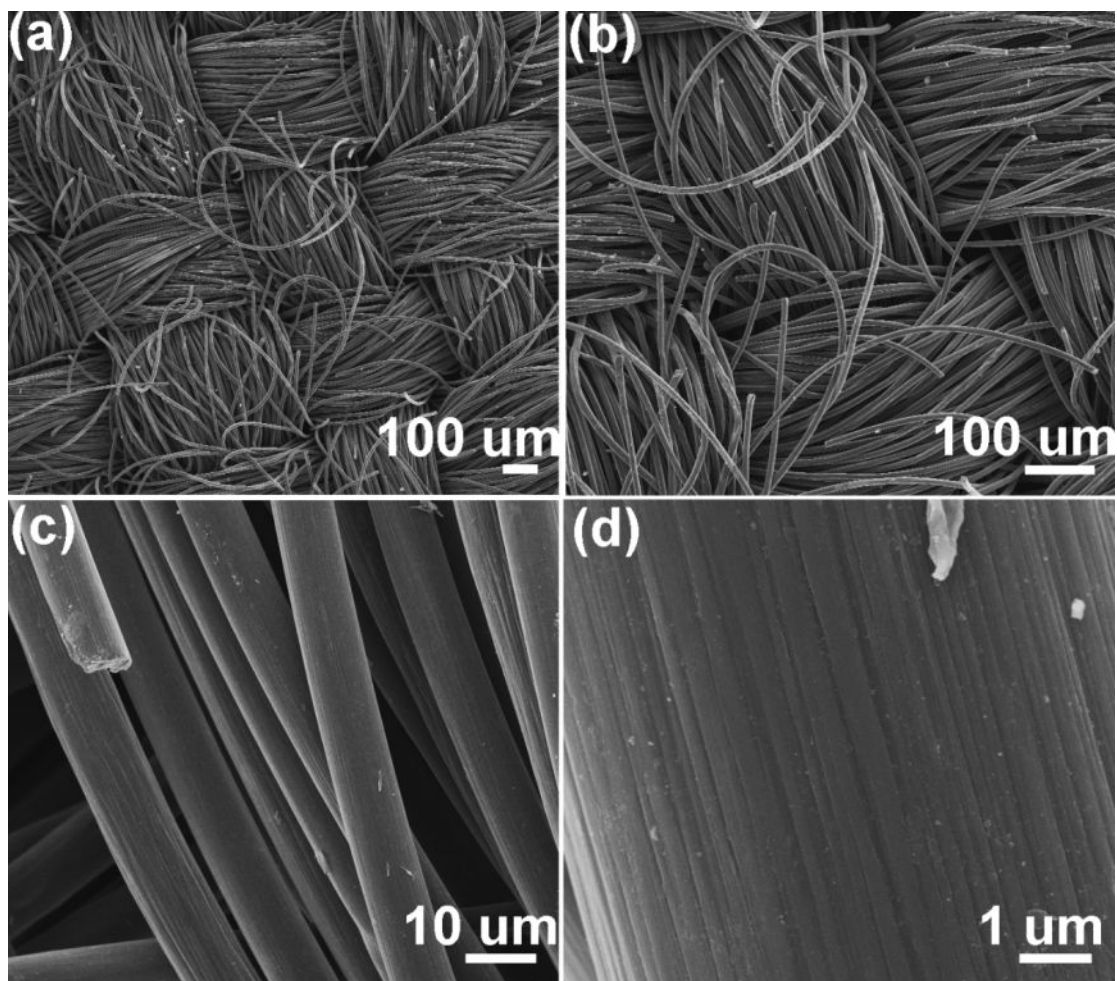
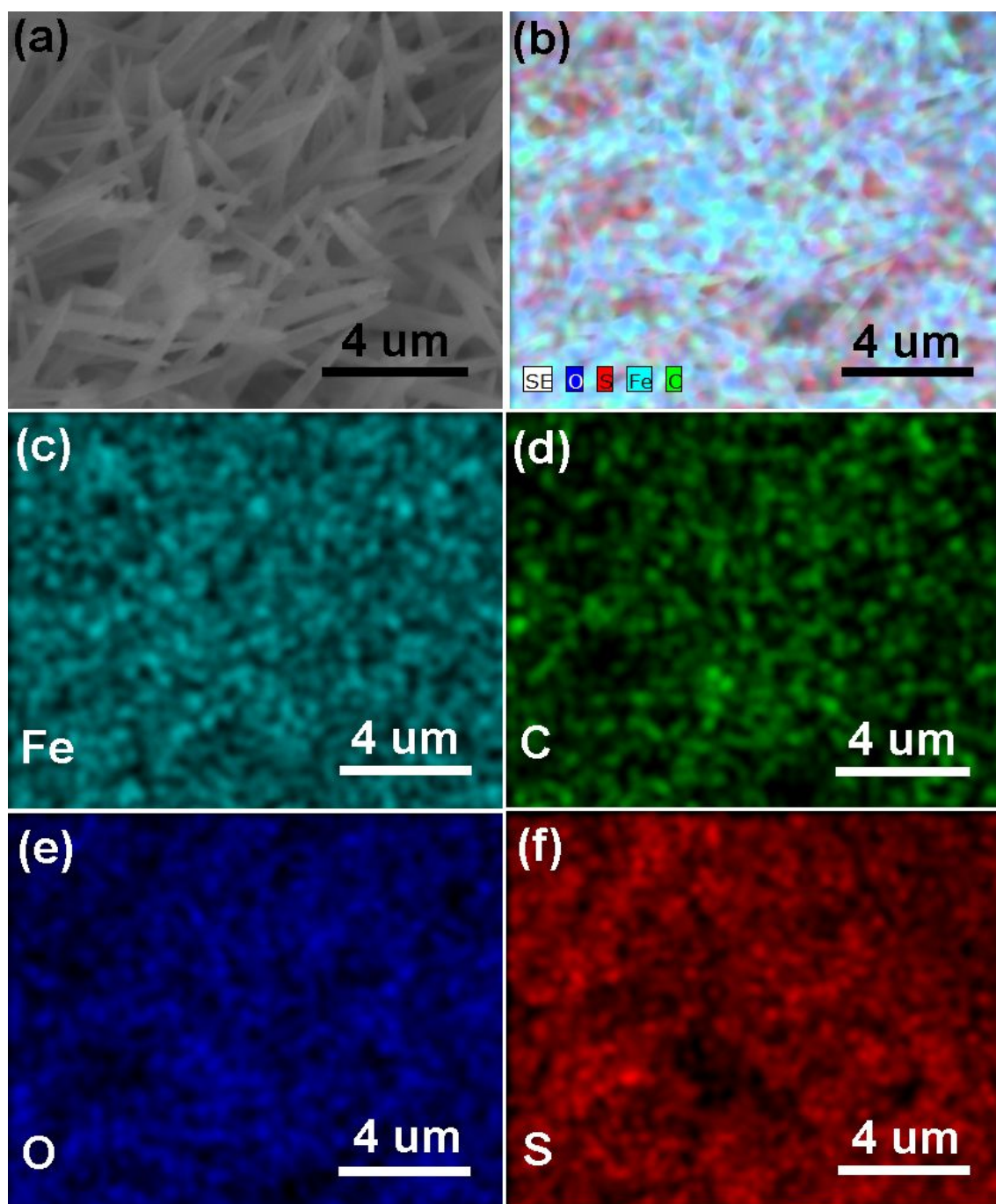**Figure S4.** Low- and high-magnification SEM images of carbon cloth (WOS 1002).

Figure S5. Element composition of the $Fe_3O_4@C@S$ cathode: (a) low-magnification image of $Fe_3O_4@C@S$; (b-f) the corresponding EDX elemental mapping images of overlap (b), iron (c), carbon (d), oxygen (e) and sulfur (f).
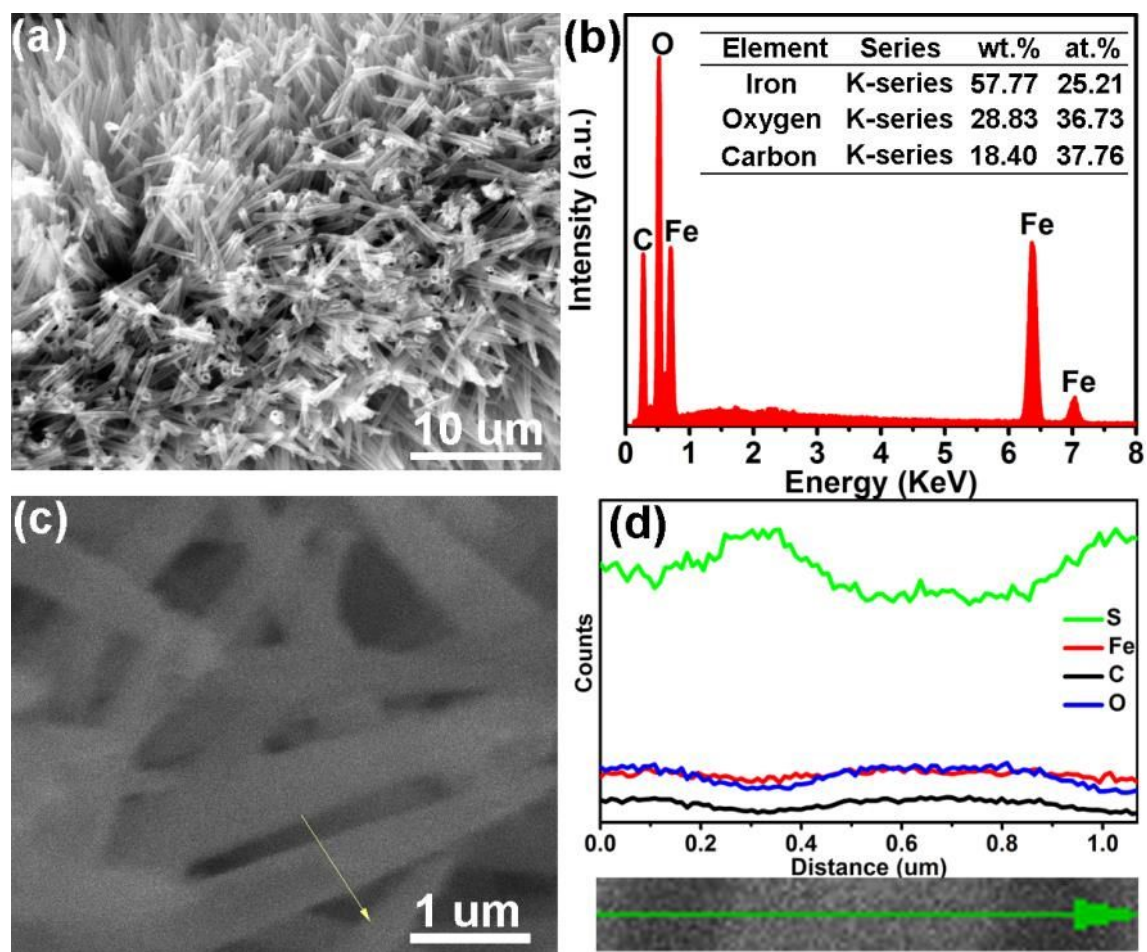
Figure S6. The elemental analysis of Fe$_3$O$_4$@C (a,b) and Fe$_3$O$_4$@C@S nanotube arrays (c,d): (a) low-magnification SEM image of Fe$_3$O$_4$@C nanoarrays; (b) the corresponding EDS spectrum of Fe$_3$O$_4$@C and the EDS data analysis of Fe$_3$O$_4$@C (insert); (c,d) high-magnification SEM image (c) and the corresponding elemental line profiles (d) across a Fe$_3$O$_4$@C@S nanotube.
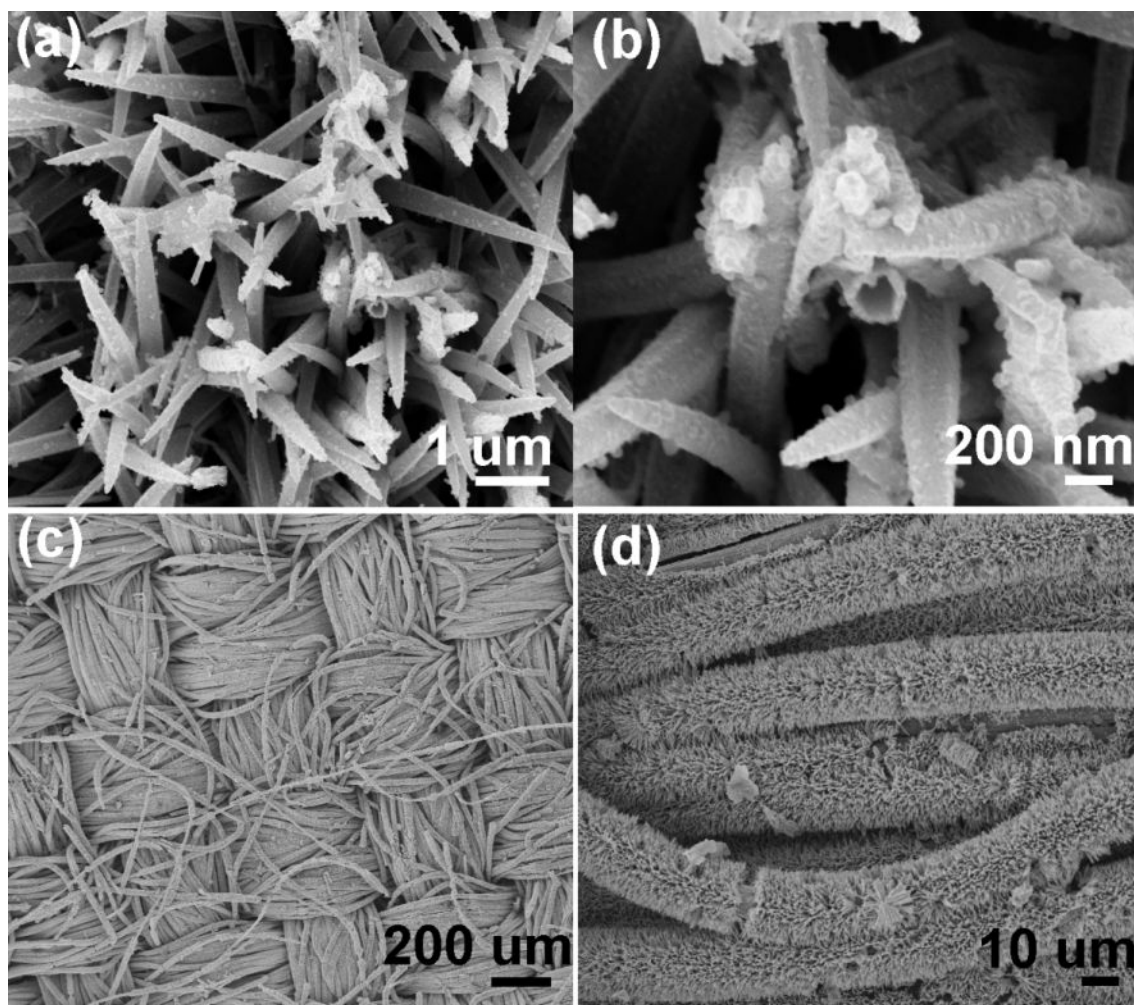
Figure S7. (a,b) Low- and high-magnification SEM images of CF/FeP@C; (c,d) low-
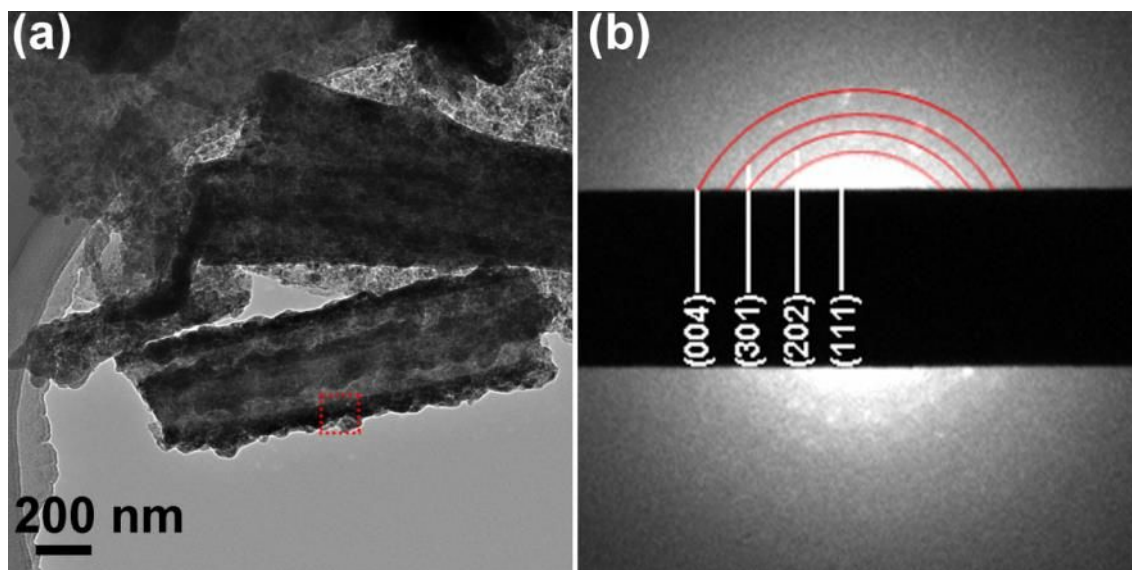
and high-magnification SEM images of CF/FeP@C@S.

Figure S8. TEM images of carbon-coated FeP nanotubes (a) the corresponding SAED pattern of a single FeP@C nanotube (b).
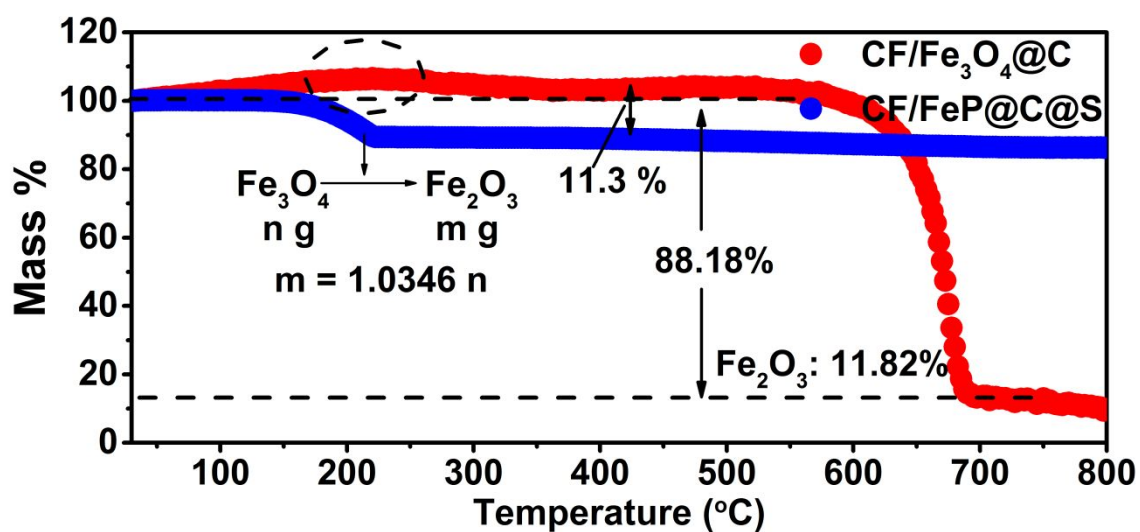

Figure S9. TGA curves of CF/Fe$_3$O$_4$@C and CF/FeP@C@S at a temperature ramp of 5 $^\circ$C min^{-1} in oxygen and argon atmosphere. According to the reaction of Fe$_3$O$_4$ with O$_2$, we can calculate the content of Fe$_3$O$_4$ in Fe$_3$O$_4$@C is 86.1%, and sulfur content in CF/FeP@C@S was 1.56 mg cm^{-2}.
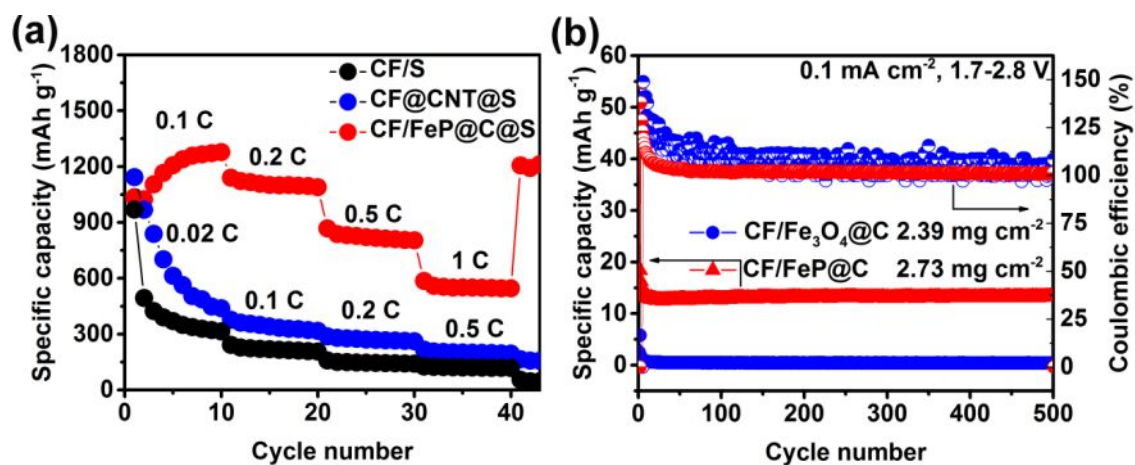
Figure S10. (a) The rate performance of CF/S, CF/CNT@S and CF/FeP@C@S; (b) Li-ion storage performances of CF/Fe$_3$O$_4$@C and CF/FeP@C at 0.1 mA cm^{-2} within the voltage window of 1.7-2.8 V.
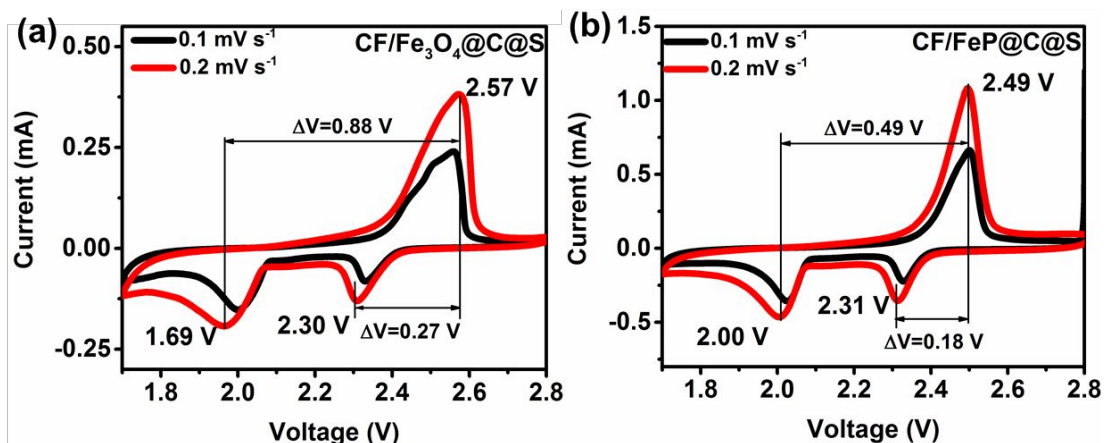
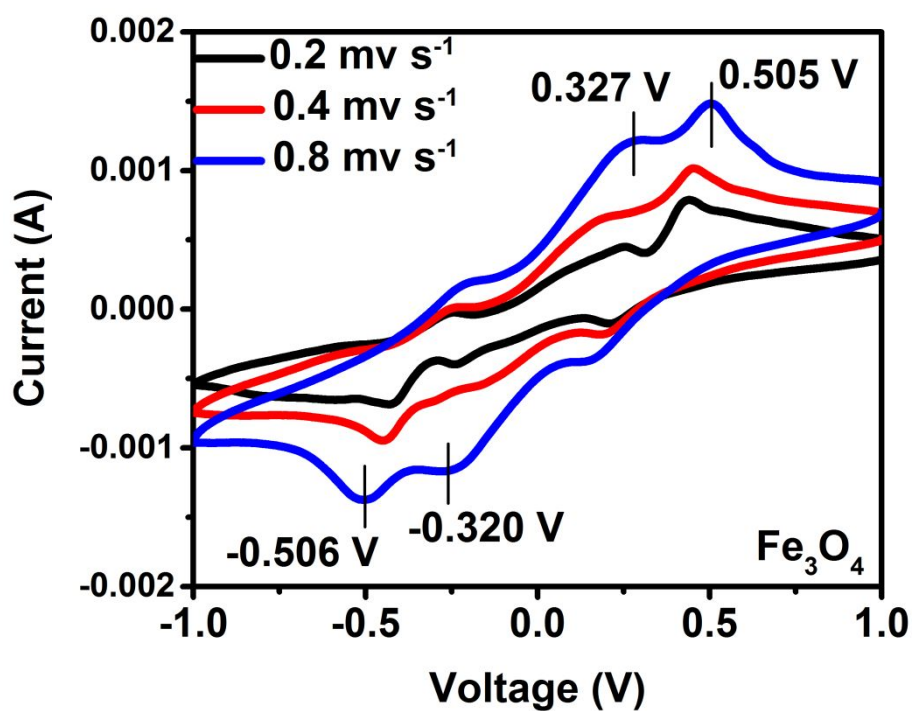**Figure S11**. CV curves of $CF/Fe_3O_4@C@S$ (a) and $CF/FeP@C@S$ (b) cathodes at sweep rates of 0.1 and 0.2 mV s^{-1}

Figure S12. CV curves of $CF/Fe_3O_4@C$ in a symmetric cell with Li_2S_4 as the electrolyte with different scan rates (0.2−1.0 mV s^{-1}).
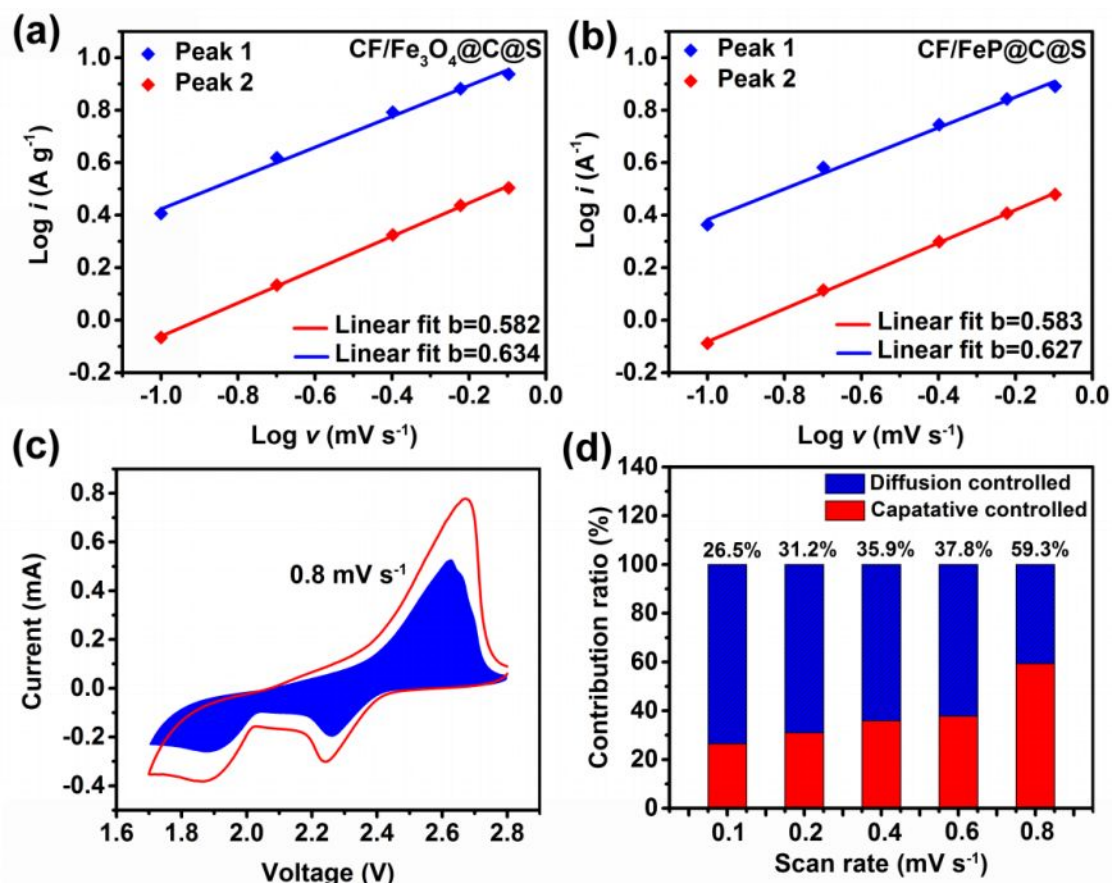
Figure S13. (a,b) The CV peak current (I_p) logarithmically potted as a function of the sweep rate (v) to give the slope of CF/Fe$_3$O$_4$@C@S (a) and CF/FeP@C@S (b); (c) the separation of the capacitive and diffusion currents at a scan rate of 0.8 mV s^{-1}; the capacitive contribution to the total current is represented by the shaded region; (d) the normalized capacity contribution ratio of the capacitive- and diffusion-controlled charge versus scan rate.
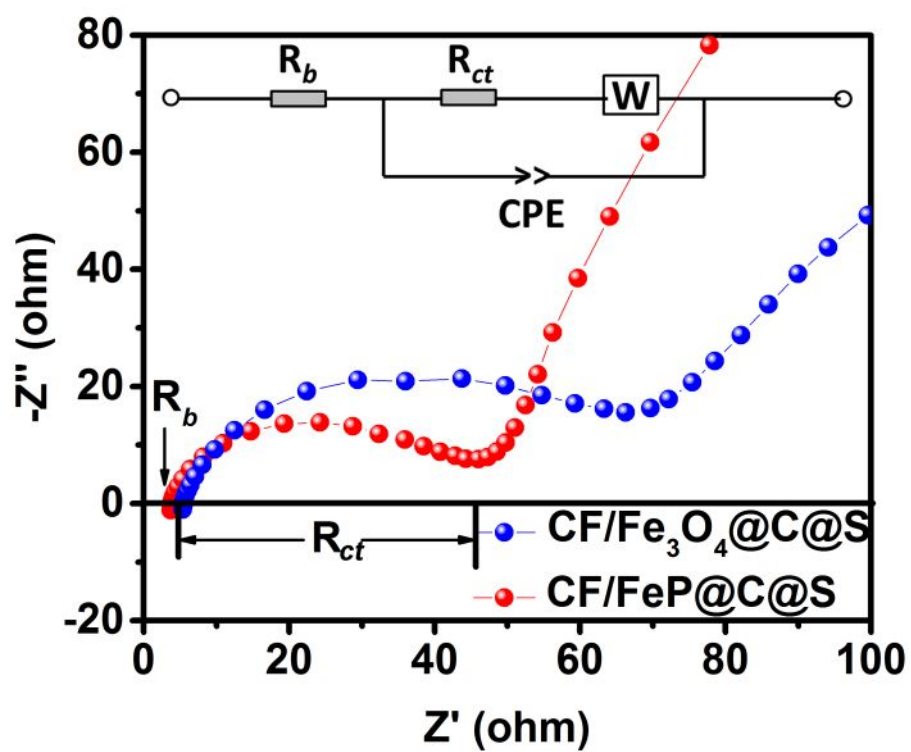
Figure S14. EIS spectra of Li-S batteries with CF/Fe$_3$O$_4$@C@S and CF/FeP@C@S as the cathode.
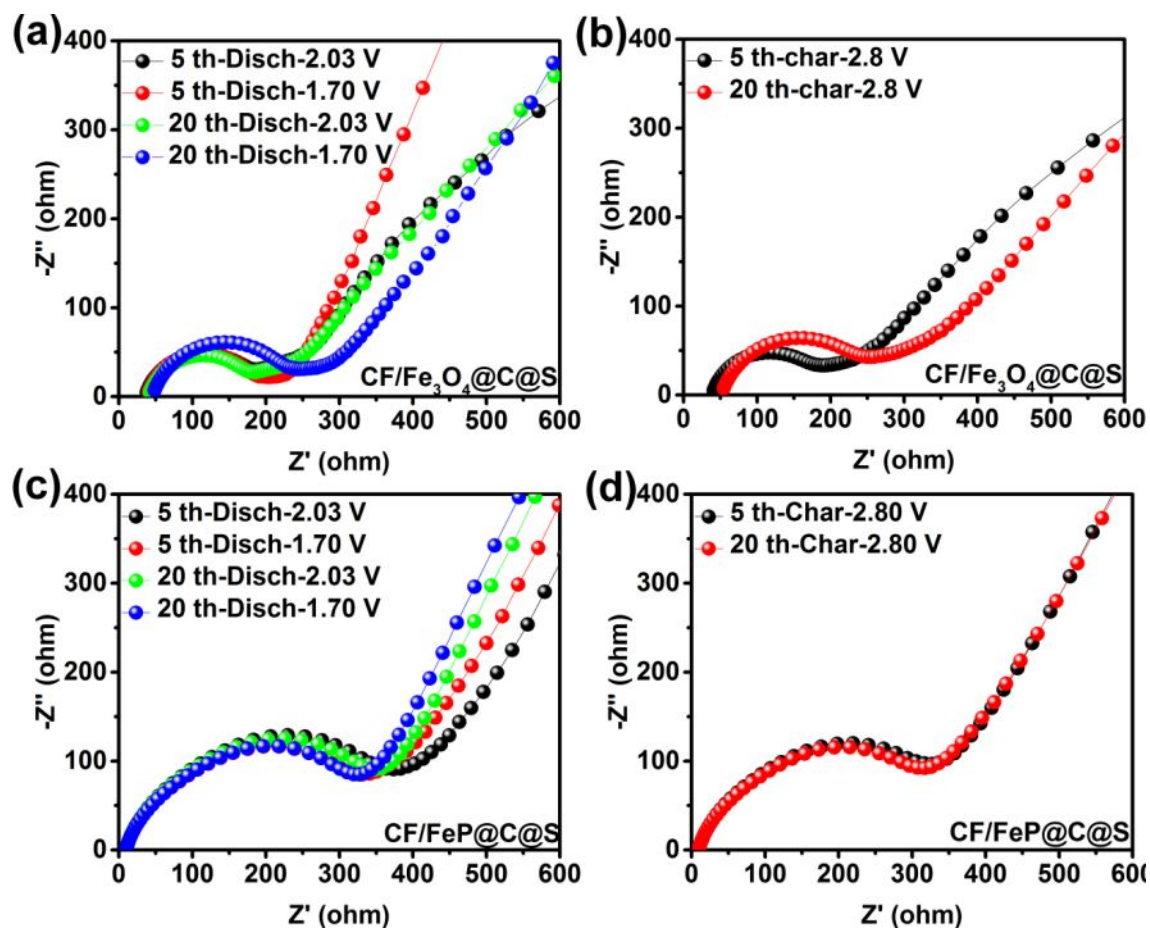
Figure S15. EIS plots of CF/Fe$_3$O$_4$@C@S (a,b) and CF/FeP@C@S (c,d) after different
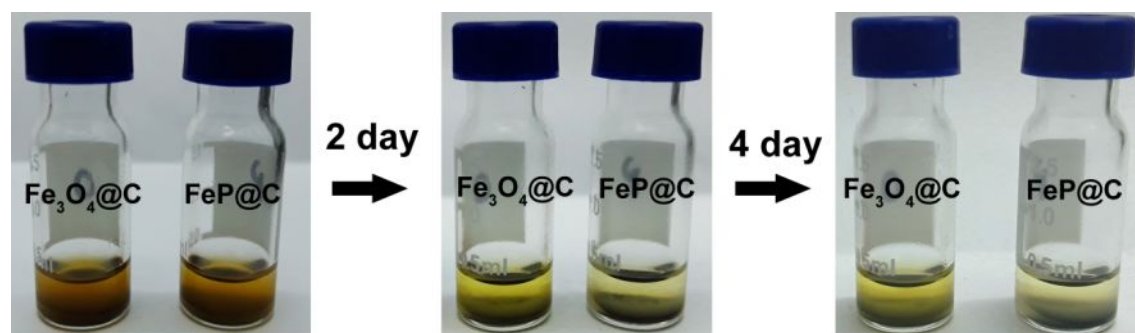
cycles at 1.0C.

Figure S16. Adsorption ability tests of CF/Fe$_3$O$_4$@C and CF/FeP@C with Li$_2$S$_4$ in four

days.
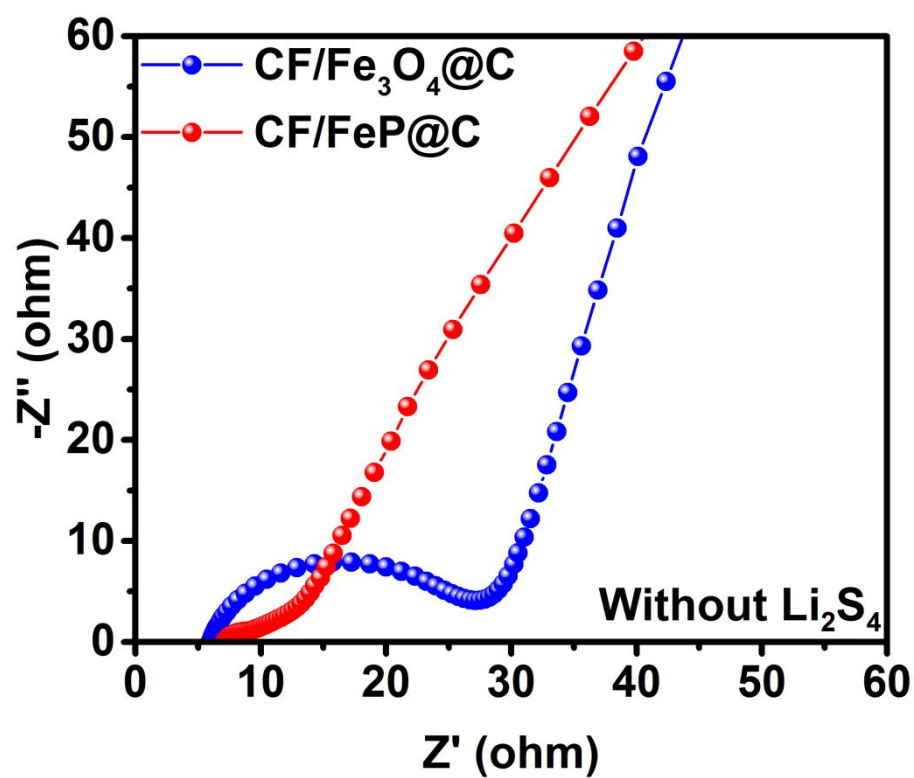
Figure S17. EIS spectra of the symmetric batteries with CF/Fe3O4@C and CF/FeP@C

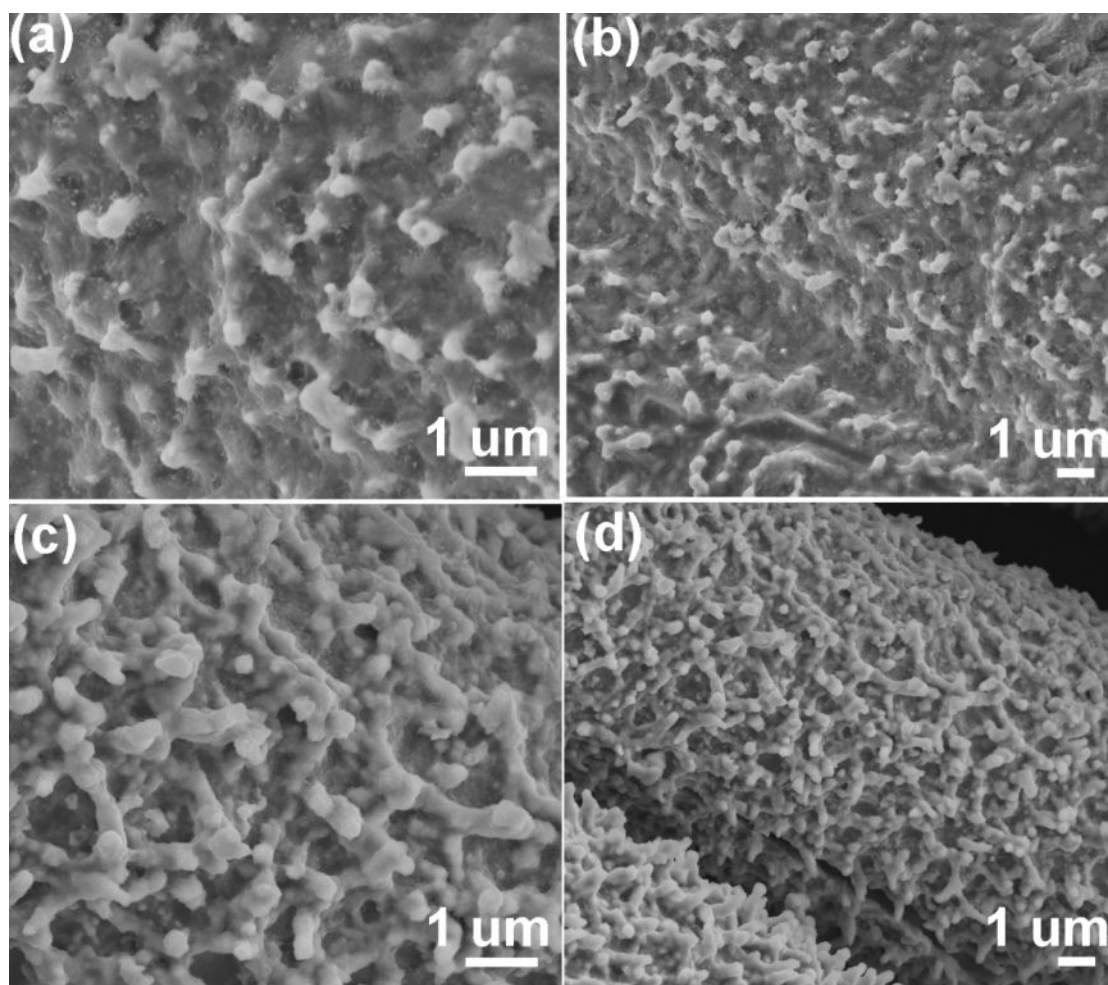as the electrode (without Li2S4 as electrolyte).

Figure S18. SEM images of CF/Fe$_3$O$_4$@C@S (a,b) and CF/FeP@C@S (c,d) after rates

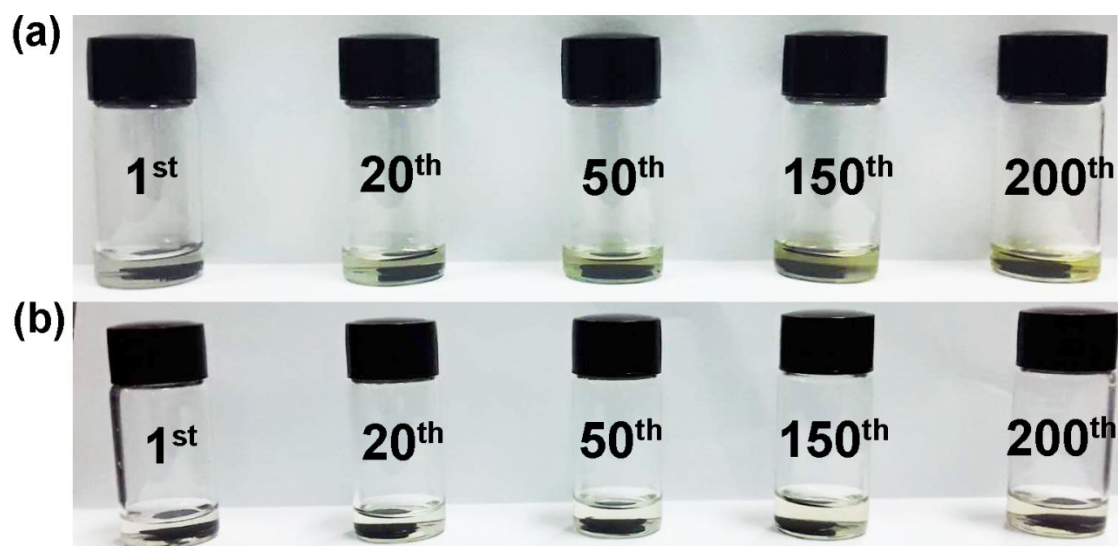performance test (0.1−1.0 C).

Figure S19. Optical images of diethyl carbonate (DEC) solutions with different cycles for CF/Fe$_3$O$_4$@C@S (a) and CF/FeP@C@S (b).

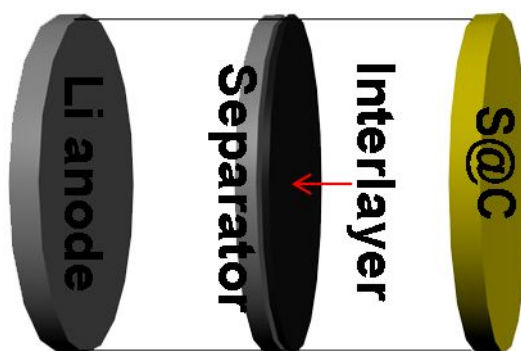**Figure S20**. The schematic structure of Li-S batteries with CF/Fe$_3$O$_4$@C and CF/FeP as the interlayer.
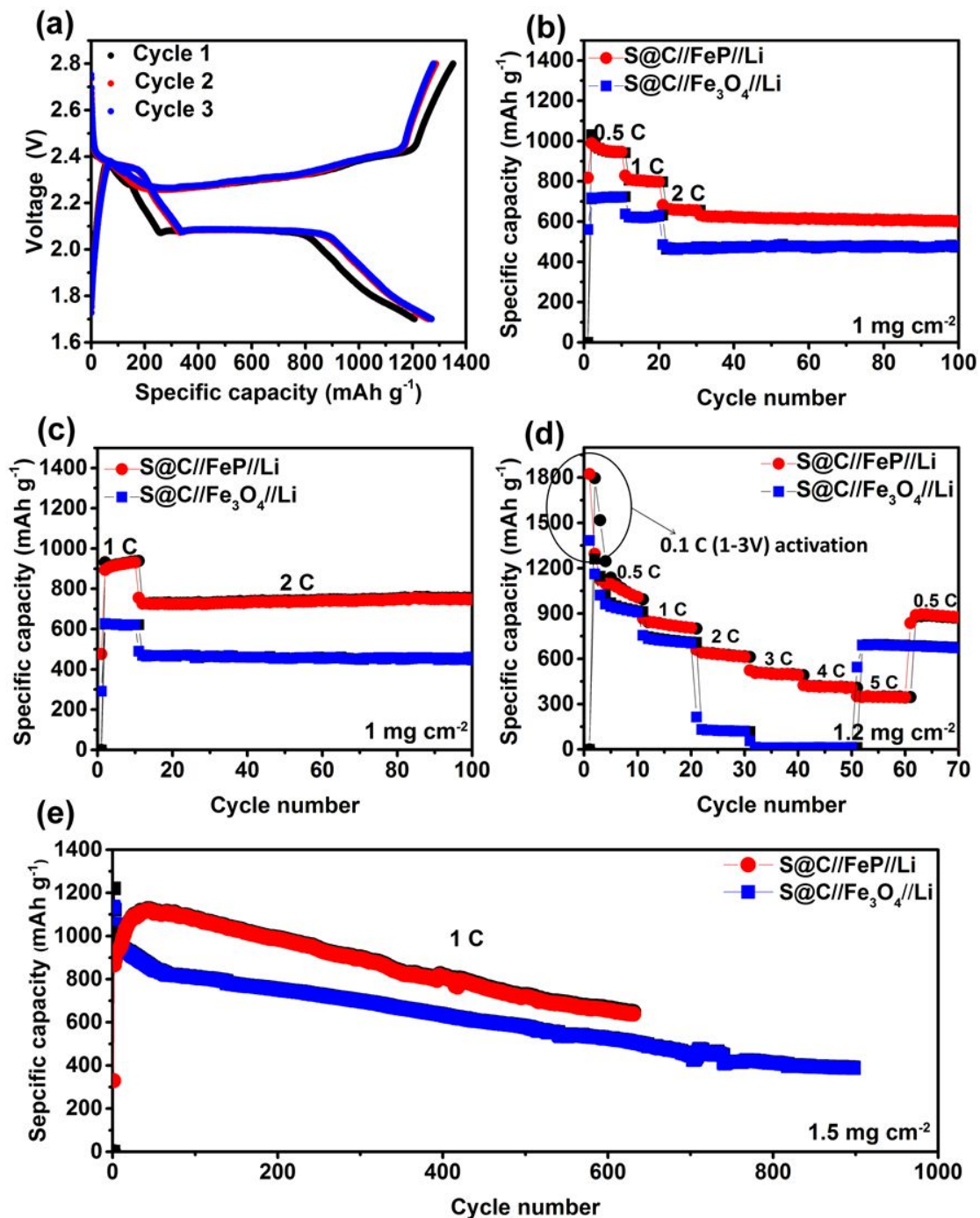
Figure S21. Detailed Li-S battery performances of CF/FeP@C and CF/Fe$_3$O$_4$@C as the interlayer for Li-S batteires: (a) the first three voltage-capacity curves at 0.1C. (b-c) the cycling performance at 2 C; (d) the rate performance at different rates (0.5−5 C); (e) the long cycling performance at 1C.
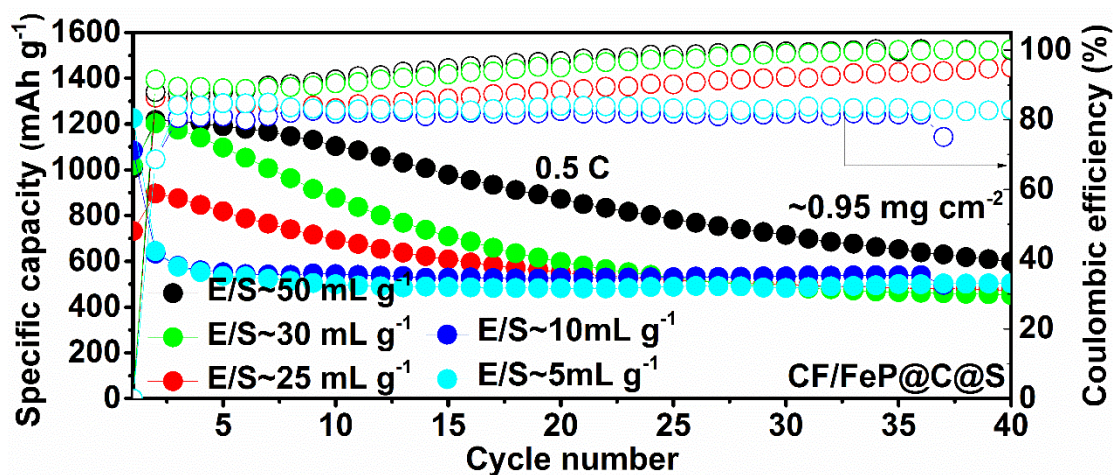
Figure S22. Comparison of the Coulombic efficiency and cycle performance of CF/FeP@C@S electrodes with different electrolyte (1.0 M LiTFSI in DME:DOL=1:1 Vol%) contents.
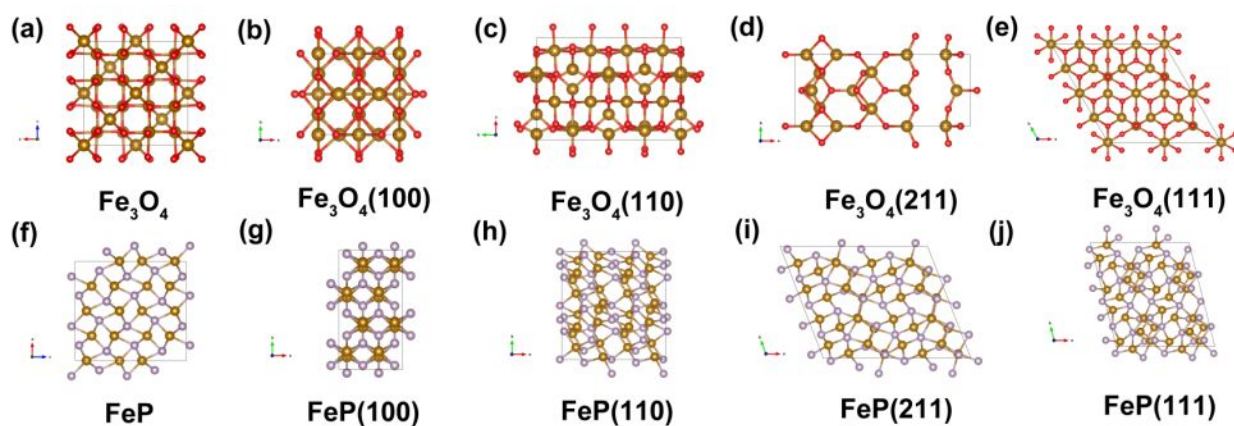
Figure S23. The geometry structures of (100), (110), (211) and (111) planes of Fe_3O_4 (a-e) and FeP (f-j).
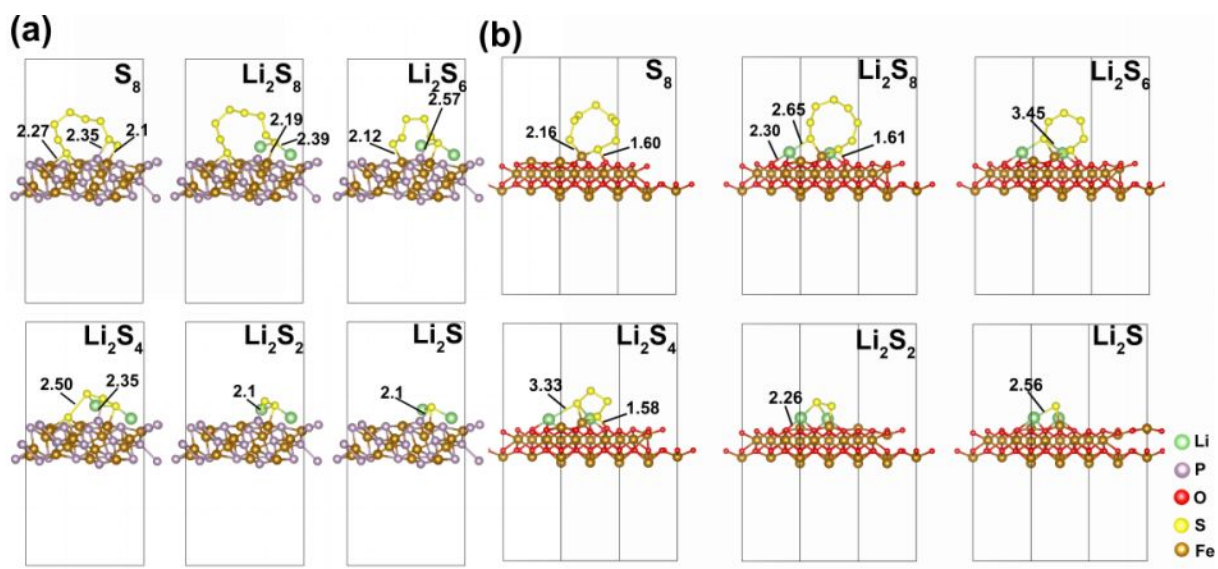
Figure S24. Adsorption configurations and energies of sulfur and LPS including Li_2S_8, Li_2S_6, Li_2S_4, Li_2S_2 and Li_2S.
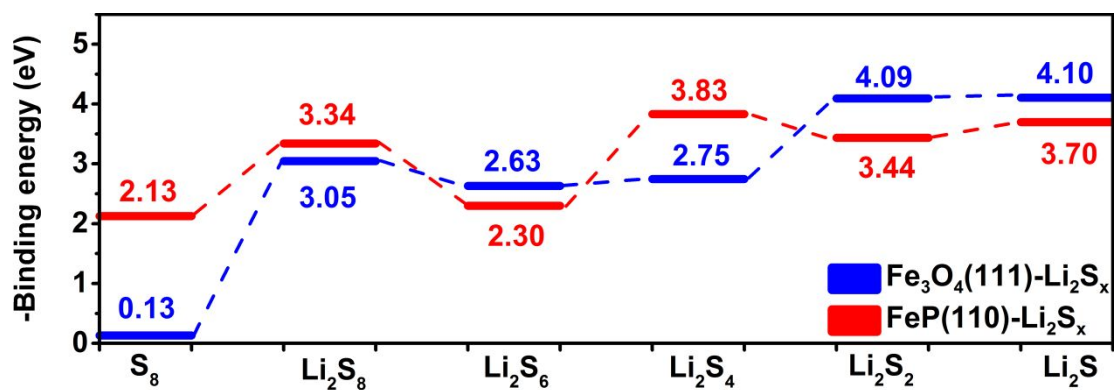
Figure S25. The binding energies of several LPS with (111) plane of Fe_3O_4 and (110) plane of FeP.
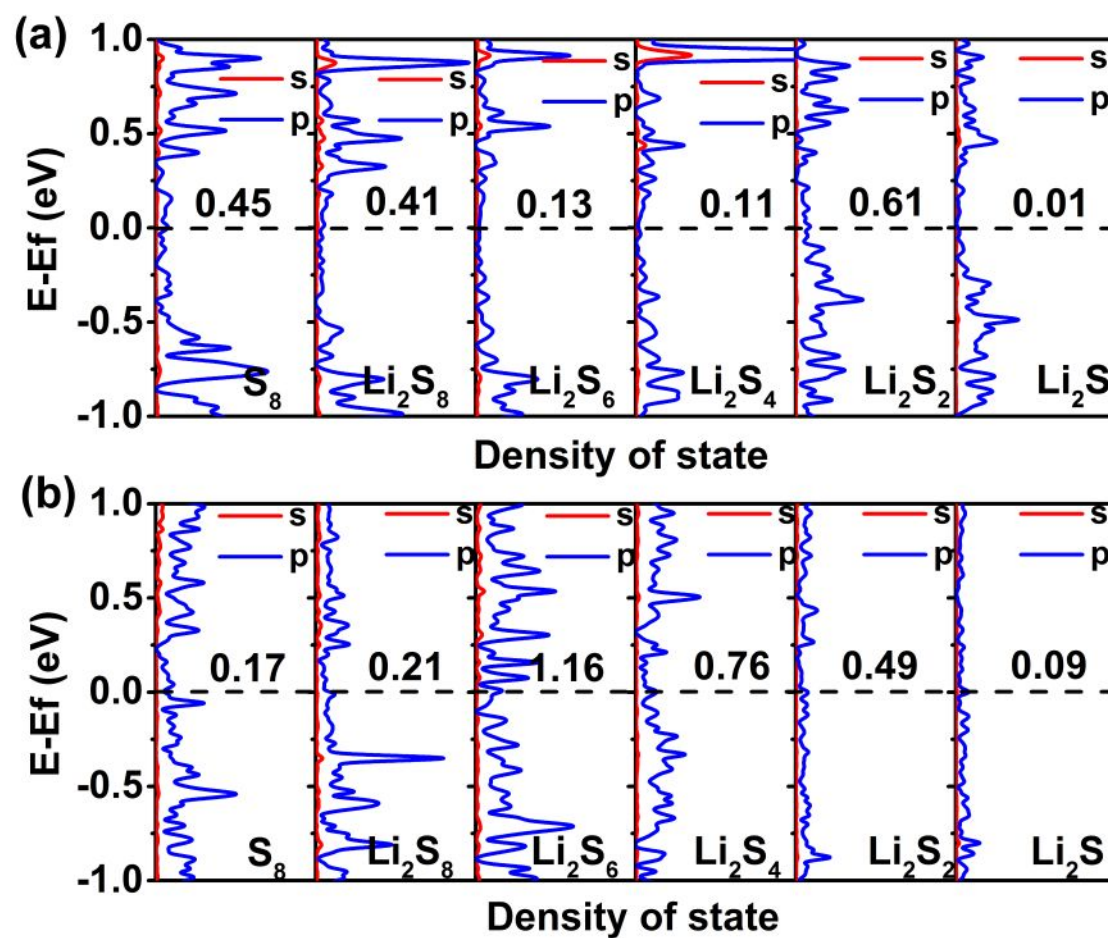
Figure S26. The density of states analysis of s and p bands of several LPS in Fe_3O_4 (a) and FeP (b) systems.

Figure S27. Surface electron density (a,c) and electron density difference (b,d) of Fe_3O_4 (a,b) and FeP (c,d).

Figure S28. The diffusion energy barriers and corresponding optimized structures of Li$_2$S and Li$_2$S$_4$ on Fe$_3$O$_4$ and FeP interfaces.

Table S1. The surface energies and atom surface densities of main lattice planes of

Fe_3O_4 and FeP crystals.

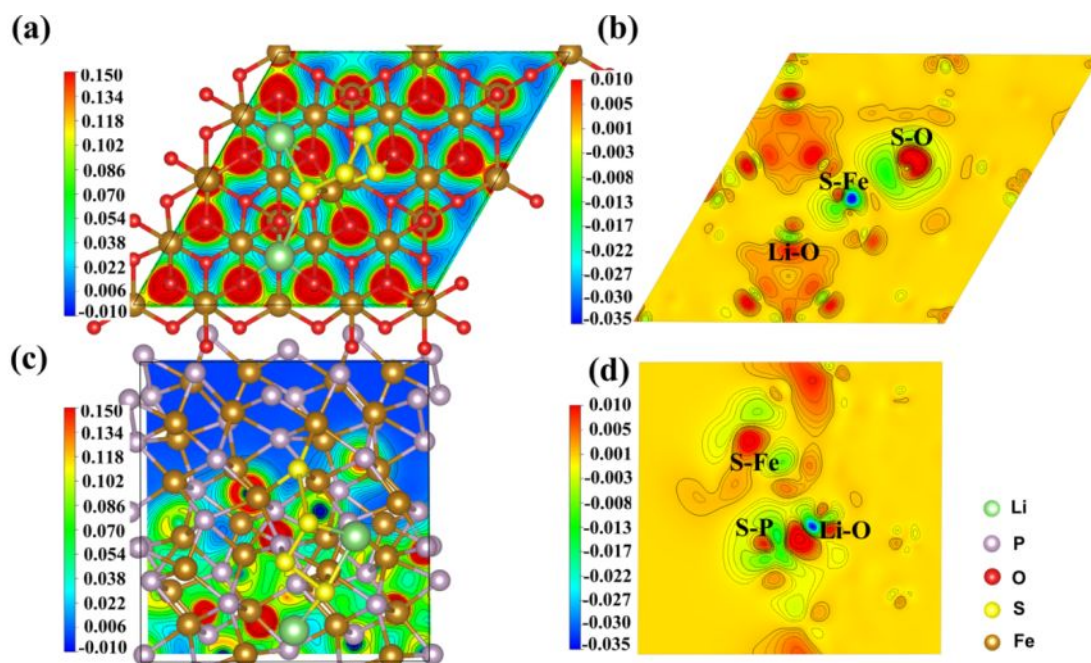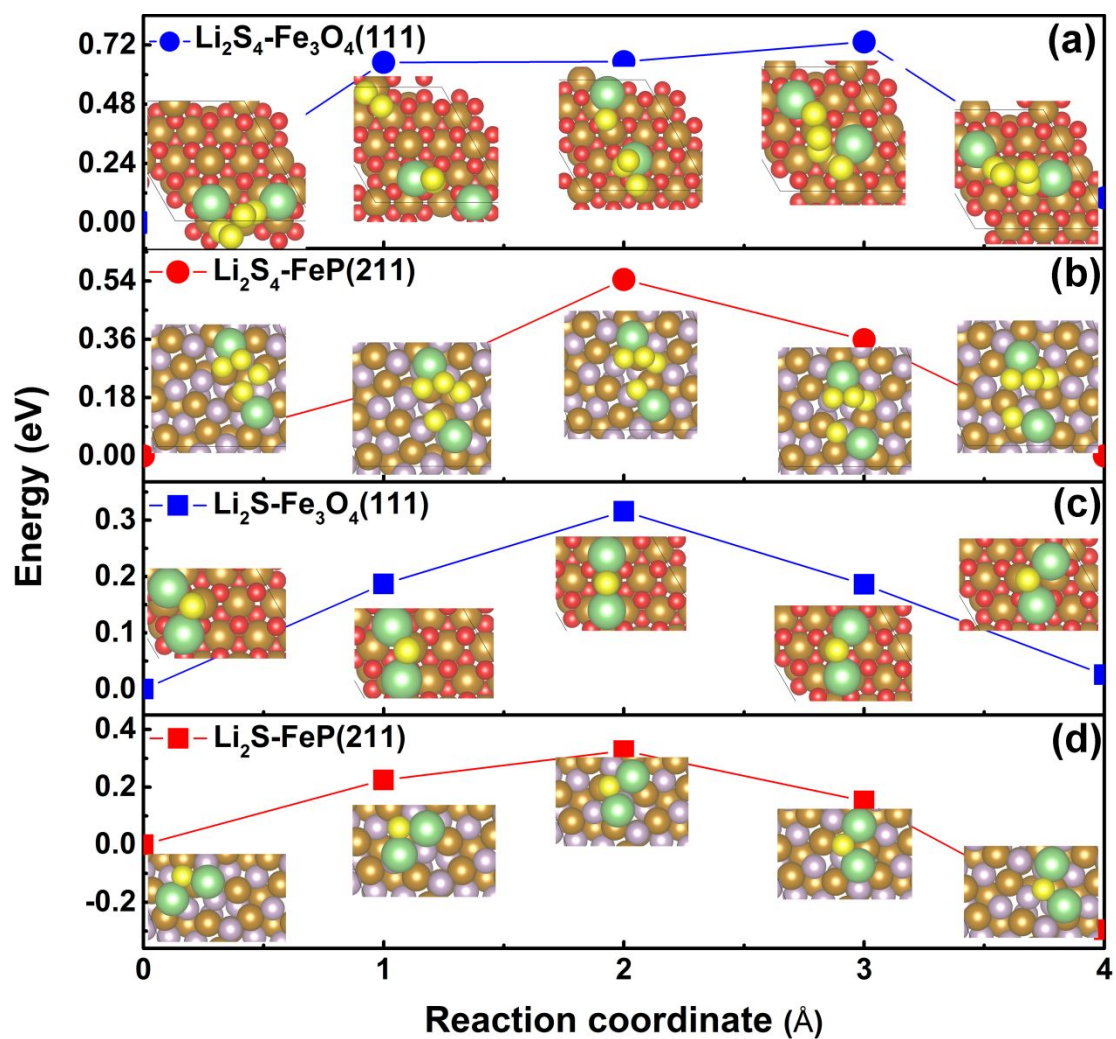| Surface	Fe_3O_4	Fe_3O_4 (100)	Fe_3O_4 (110)	Fe_3O_4 (111)	Fe_3O_4 (211)
E_{sur} (eV)	-	0.0436	0.0488	0.0320	0.0468
D_{atom}	-	0.1136	0.2009	0.2050	0.1623
Surface	FeP	FeP (100)	FeP (110)	FeP (111)	FeP (211)
E_{sur} (eV)	-	0.1771	0.1248	0.1569	0.0977
D_{atom}	-	0.1393	0.1719	0.1608	0.1455

The specific surface energies were calculated with the formula: $E_{sur} = (E_{slab} - n\,E_{bulk})/2A$,

where E_{slab} is the energy of the slab, E_{bulk} is the energy of a unit cell, n is the number of

unit cells and A is the area of the surface; atom surface densities were calculated with

the formula $D_{atom} = n/A$, n is number of atoms in the slap.

Table S2. The EIS fitting data of CF/Fe$_3$O$_4$@C@S and CF/FeP@C@S cathodes at different discharge stages.

Batteries cycle numbers (Discharge to 2.03 V)	CF/Fe$_3$O$_4$@C@S		CF/FeP@C@S	
	R_b	R_{ct}	R_b	R_{ct}
Without cycling	6.84	75.82	3.49	42.06
After 5 cycles	44.59	138.2	13.6	200.7
After 20 cycles	49.1	131.6	13.67	206.2
Batteries cycle numbers (Discharge to 1.70 V)	CF/Fe$_3$O$_4$@C@S		CF/FeP@C@S	
	R_b	R_{ct}	R_b	R_{ct}
After 5 cycles	46.51	134	13.65	203.4
After 20 cycles	57.34	176.7	13.4	182.7
Batteries cycle numbers (Charge to 2.8 V)	CF/Fe$_3$O$_4$@C@S		CF/FeP@C@S	
	R_b	R_{ct}	R_b	R_{ct}
After 5 cycles	47.56	134.7	13.18	163.7
After 20 cycles	63.75	177.6	13.17	161.5

Table S3. The EIS fitting data of $CF/Fe_3O_4@C$ and $CF/FeP@C$ symmetric cells with/without Li_2S_4 solution.

With/without Li_2S_4	$CF/Fe_3O_4@C$		$CF/FeP@C$	
	R_b	R_{ct}	R_b	R_{ct}
With Li_2S_4	11.59	25.54	10.11	13.43
Without Li_2S_4	6.329	14.57	7.154	1.324